XIII. DSIF Operations

OPERATIONS AND FACILITIES

A. Radio Science Support, *T. Sato, L. Skjerve, and D. Spitzmesser*

1. RAES Panel Activities

The Radio Astronomy Experiment Selection (RAES) panel has completed review of three proposals, and each proposal received a favorable evaluation. Table 1 contains a general summary of these experiments. At the present time, the panel is reviewing three new proposals.

2. Radio Science Operations

Since May 1, 1970, five radio science experiments have been supported at DSN facilities. Outlines of these experiments are given below:

a. SCO-XR1 observations. As reported in SPS 37-63, Vol. II, pp. 98–100, Dr. C. S. Boyer, University of California at Berkeley, submitted a proposal to the RAES panel to conduct extensive observations of the 13-cm radio emissions from SCO-XR1, an X-Ray source in the constellation Scorpio. The objective of the experiment is to determine if the radio emissions from this object are variable and correlated with previously observed optical variability. The observations were conducted in May and June of 1970 at DSS 14.

Since the radio emissions from this object are very weak, a stabilized radiometer (*Subsection VI-C*) developed by the Telecommunications Division was employed, which considerably enhanced the probability of a successful experiment.

b. Trans-Pacific very long baseline interferometer experiment. On June 13, 1970, Drs. A. Moffet (associated with Owens Valley Radio Observatory) and D. Robertson (principal officer of Space Research Group, Weapons Research Establishment, Adelaide, Australia) conducted another 24-h trans-Pacific very long baseline interferometer (VLBI) experiment between the Goldstone DSCC in California and the Canberra DSCC in Australia (SPS 37-62, Vol. II, pp. 125–127). This was the first observation under the auspices of the RAES panel (SPS 37-63, Vol. II, pp. 99–100). During the experiment, which was supported by DSSs 12, 14, and 42, data was taken on 29 radio sources. The data tapes are now being evaluated by the experimenters.

Table 1. Approved experiments

Experimenter	Affiliation	Objective	Comments
Dr. A. Moffet	Owens Valley Radio Observatory	To detect pulsar emissions at 7840 MHz	Experiment completed
Dr. A. Moffet	Owens Valley Radio Observatory	To study polarization characteristics of pulsar emissions at 2295 MHz	Scheduled for Fall 1970
Dr. B. Burke	Massachusetts Institute of Technology	To conduct a precision test of general relativity by use of very long baseline interferometry	Scheduled for October 1–15, 1970
Dr. T. Clark	Goddard Space Flight Center		
Dr. R. Goldstein	Jet Propulsion Laboratory		
Dr. A. Rogers	Haystack Radio Observatory		
Dr. I. Shapiro	Massachusetts Institute of Technology		

c. X-Band pulsar observations. An experimental low-noise X-band feed cone (SPS 37-62, Vol. II, p. 80) was part of the tricone feed assembly installed at DSS 14 early this year. An experiment to study X-band emissions of pulsars using this new experimental capability, was conducted on July 4, 1970, and data was obtained. The principal investigator was Dr. A. Moffet.

d. X-Band planetary radar. Two X-band planetary radar experiments were conducted jointly with MIT's Lincoln Laboratory in May, June, and July 1970. The first experiment attempted to obtain a radar return from Venus and from Callisto, a satellite of Jupiter. Lincoln Laboratory's Haystack Facility radiated 300 kW at the target and DSS 14 attempted to receive the return. The received data were transmitted via microwave to DSS 13 for post-reception processing. Runs were made on six evenings in May and June. The data has not been fully evaluated at this time.

The second experiment was an attempt to radar-range the planet Mercury near superior conjunction. This experiment was designed as a test of general relativity. The observations, utilizing the same facilities as the Callisto experiment, were conducted over a 3-wk period in June and July 1970. The data is still being evaluated.

This combination of facilities represented the most powerful planetary radar system employed to date in the world.

B. Computerized Receiver and Telemetry SNR Predictions Program, *W. Porché*

1. Introduction

A computerized program has been developed to provide in one document, predicted receiver signal strength, receiver margin, predicted telemetry ST_b/N_0, and parity error rate or bit error rate. The program Receiver and Telemetry SNR Predictions is used to generate predicts for *Mariner* and *Pioneer* spacecraft.

The receiver and telemetry SNR predictions program is presently being used by the real and non-real time analysis groups, operations engineering, and system data analysis personnel. These predictions are sent to the various tracking stations and are used by the stations to ascertain normal operation of the telemetry system.

2. Operation

Figure 1 is a listing of the program output. This listing is obtained through the following data inputs and program functions:

a. Identification input. The ID card provides the following inputs:

Modulation index
System noise temperature

Receiver bandwidth
Antenna polarizer in or out
85- or 210-ft network
Spacecraft number
Month to start predicts
Day of month to start predicts
Year to start predicts
Pass number to start predicts
Number of days to run predicts
Mission (*Pioneer* or *Mariner*)
Telemetry mode (single or dual station)

b. Data input. Data input is by cards providing day of year and spacecraft range in kilometers. The range data is obtained from the spacecraft trajectory printout.

c. Temperature input. The temperature card is used when dual-station telemetry is to be output. The system noise temperature is provided for stations operating in the dual-telemetry mode.

d. Range interpolation. The program uses a four-point La Grange interpolation routine. The day of year and spacecraft range is input to the program and interpolated to provide range for daily computations. The program will take up to 99 inputs and can compute predicts for 999 days.

e. Prediction computations. The equation for free-space loss (Ref. 1) is

$$L_{fs} = 92.45 + 20 \log (f) + 20 \log (d)$$

PIONEER 8 RECEIVER AND TELEMETRY SNR PREDICTIONS. 85 FOOT NETWORK

DUAL STATION-COMBINED TELEMETRY MODE

RECEIVER BANDWIDTH = 3.0 HERTZ
SYSTEM NOISE TEMPERATURE:
DSS 11 = 40.00 DEGREES K
DSS 12 = 17.00 DEGREES K
DSS 61 = 42.00 DEGREES K
DSS 62 = 30.00 DEGREES K
POLARIZER IN OR OUT = IN
BAD PER = ******
SNR=ST/NO
MODULATION INDEX = 51.60 DEGREES

DATE	DAY	PASS NO.	RECEIVER SIGNAL STRENGTH	DEEP SPACE STATIONS	PARITY ERROR RATE(PER) 8BPS	16BPS	64BPS	TELEMETRY SNR 8BPS	16BPS	64BPS
6- 1-70	152	902	-164.10	DSS 11/12	.00000	.00000	******	13.36	10.78	5.03
				DSS 61/62	.00000	.00568	******	11.69	9.12	3.37
6- 2-70	153	903	-164.11	DSS 11/12	.00000	.00000	******	13.34	10.77	5.01
				DSS 61/62	.00000	.00585	******	11.67	9.10	3.35
6- 3-70	154	904	-164.13	DSS 11/12	.00000	.00000	******	13.32	10.75	5.00
				DSS 61/62	.00000	.00602	******	11.66	9.09	3.33
6- 4-70	155	905	-164.15	DSS 11/12	.00000	.00000	******	13.31	10.73	4.98
				DSS 61/62	.00000	.00619	******	11.64	9.07	3.32
6- 5-70	156	906	-164.16	DSS 11/12	.00000	.00000	******	13.29	10.72	4.96
				DSS 61/62	.00000	.00636	******	11.62	9.05	3.30
6- 6-70	157	907	-164.18	DSS 11/12	.00000	.00000	******	13.27	10.70	4.95
				DSS 61/62	.00000	.00653	******	11.61	9.03	3.28
6- 7-70	158	908	-164.20	DSS 11/12	.00000	.00000	******	13.25	10.68	4.93
				DSS 61/62	.00000	.00671	******	11.59	9.02	3.27
6- 8-70	159	909	-164.22	DSS 11/12	.00000	.00000	******	13.24	10.66	4.91
				DSS 61/62	.00000	.00688	******	11.57	9.00	3.25
6- 9-70	160	910	-164.23	DSS 11/12	.00000	.00000	******	13.22	10.65	4.90
				DSS 61/62	.00000	.00706	******	11.56	8.98	3.23
6-10-70	161	911	-164.25	DSS 11/12	.00000	.00000	******	13.20	10.63	4.88
				DSS 61/62	.00000	.00724	******	11.54	8.97	3.22
6-11-70	162	912	-164.27	DSS 11/12	.00000	.00000	******	13.19	10.61	4.86
				DSS 61/62	.00000	.00741	******	11.52	8.95	3.20

Fig. 1. Two-station dual telemetry predictions

where

L_{fs} = free space loss, dB

f = received frequency, GHz

d = spacecraft range, km

The predicted received signal strength is computed as follows:

SS = (spacecraft gain) + (ground antenna gain) − (modulation loss) − L_{fs} − (antenna pointing loss = 0.5 dB)

where the spacecraft gain

PN-6 = +48.9 dB

PN-7 = +48.2 dB

PN-8 = +49.1 dB

PN-9 = +49.1 dB

Ground antenna gain for

85-ft antenna = +53.3 dB

210-ft antenna = +61.4 dB

Modulation loss is 10 log (modulation index); the modulation index is 51.6 deg for PN-6 through 9. The modulation index for the *Mariner* spacecraft is variable. The receiver margin M, (Ref. 2) is computed by

$$M = SS - \left[10 \log\left(\frac{KT_s(BW)}{10^3}\right)\right]$$

The ST_b/N_0 of the telemetry (Ref. 2) is computed by

$DP = SS + 20 \log \tan$ (modulation index)

$$SNR = \frac{DP}{KT_s(BR)} - \text{loss}$$

where

M = receiver margin, dB

DP = telemetry data power, dB

SS = predicted receiver signal strength, dBmW

SNR = telemetry $\frac{ST_b}{N_0}$

K = Boltzmann constant

T_b = 1/bit rate

T_s = system noise temperature, °K

BW = receiver bandwidth, Hz

$KT_s = N_0$ = noise

BR = telemetry bit rate

Loss = fixed system loss depending on bit rate

Output is available for single-station telemetry or the dual-station combined-telemetry mode of operation. Dual-station combined-telemetry tracking by DSSs 11 and 12, and DSSs 61 and 62 have been experimentally tried and determined to have a definite improvement in telemetry performance. The theoretical maximum improvement for combined telemetry of two stations of equal gain is 3 dB (SPS 37-63, Vol. III, pp. 116–120). The computer program computes the dual-station combined-telemetry SNR as follows:

$$SNT = SNR_l + 10 \log\left(1 + \frac{T_l}{T_h}\right)$$

where

SNT = total SNR for combined telemetry

SNR_l = SNR of lowest system noise temperature station

T_l = lowest system noise temperature, °K

T_h = highest system noise temperature, °K

$$T_l \leq T_h \text{ and } \left(1 + \frac{T_l}{T_h}\right) \leq 2$$

Figure 1 provides an illustration of the output listing for dual-station combined telemetry. The predictions are printed for each day at 00:00 GMT. Currently, these predictions are being used by all stations in the Deep Space Network.

References

1. *Reference Data for Radio Engineers,* pp. 34-3, McGraw-Hill Book Co. Inc., New York, 1949.

2. *Deep Space Network/Flight Project Interface Design Handbook,* DSN Standard Practice 810-5, pp. 2-32 to 2-78, Jet Propulsion Laboratory, Pasadena, Calif., March 1, 1970.

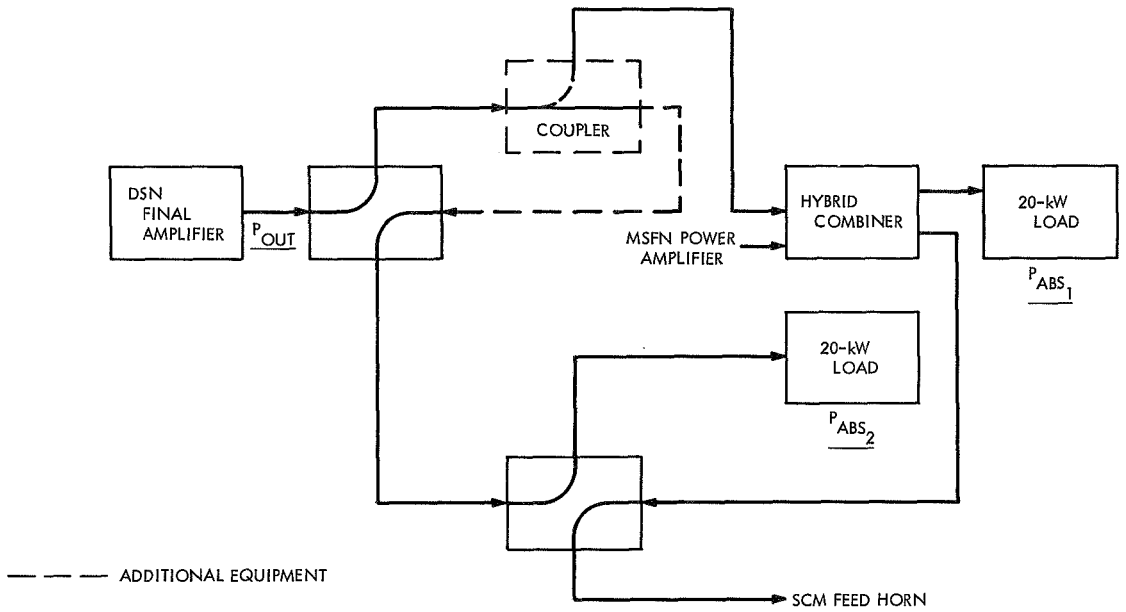

COUPLER FACTOR, dB	P_{ABS_1}, W	P_{ABS_2}, W	P_{ANT}, W
30	10	19,980	10
20	100	19,800	100
10	1000	18,000	1000

P_{ANT} = RADIATED POWER
MAXIMUM P_{ANT} = 20 kW
P_{OUT} = 20 kW (CONSTANT)

Fig. 1. Directional coupler in an 85-ft-diam antenna mutual station using combiner in attenuated RF path

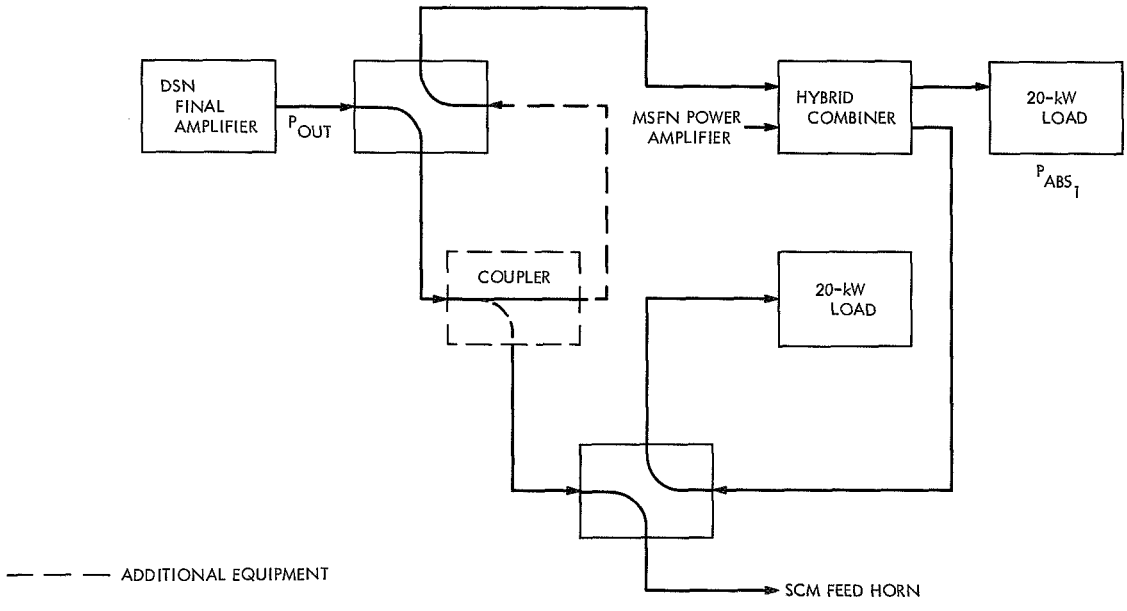

COUPLER FACTOR, dB	P_{ABS_1}, W	P_{ABS_2}, W	P_{ANT}, W
30	9990	9990	20
20	9900	9900	200
10	9000	9000	2000

P_{ANT} = RADIATED POWER
MAXIMUM P_{ANT} = 10 kW
P_{OUT} = 20 kW (CONSTANT)

Fig. 2. Directional coupler in an 85-ft-diam antenna mutual station

C. Low Transmitted Power Operation,

R. L. Riggs

1. Introduction

This report describes a method by which the radiated output power level from a DSIF antenna may be adjusted while maintaining the transmitter at constant power and bandwidth levels. The constant power output from the transmitter is split into appropriate levels between a dissipative load and the antenna feed horn.

Two devices accomplish the splitting. One device is basically a fixed high-power directional coupler (or combination of couplers), and the other device is a high-power microwave power divider that has a capability of being continuously variable.

Current instrumentation techniques for monitoring the output power level are not changed with either device, and the overall accuracy of the system is degraded only by the tolerances in the calibration of the added device(s).

2. Description

a. Fixed high-power directional couplers. In an 85-ft-diam antenna mutual station there are many possible configurations with directional couplers. These different configurations will give various combinations of antenna output power. Figures 1 and 2 illustrate two possible configurations of a mutual station, and Fig. 3 is one of a standard station. It should be noted that the 85-ft mutual station has a 20-kW transmitter and the standard station has only a 10-kW capability.

It can be seen that the output power range is dependent upon the use and coupling factor of the directional coupler. In all of the illustrations, it is assumed that the final amplifier output power is held constant at its maximum rated level.

b. High-power microwave power divider. A major problem with the use of directional couplers just described is the lack of flexibility in adjustment of output power. A directional coupler is designed to have a fixed coupling factor, and the antenna output power may vary in a continuous fashion by varying the final amplifier output power. This may lead to a degradation of transmitter stability and bandwidth characteristics.

A new device is described[1] where the power is split in any proportion between two output ports. This new device may be installed in place of the fixed directional

[1]Kolbly, R. B., *High Power Microwave Divider Concept*, May 1970 (JPL internal document).

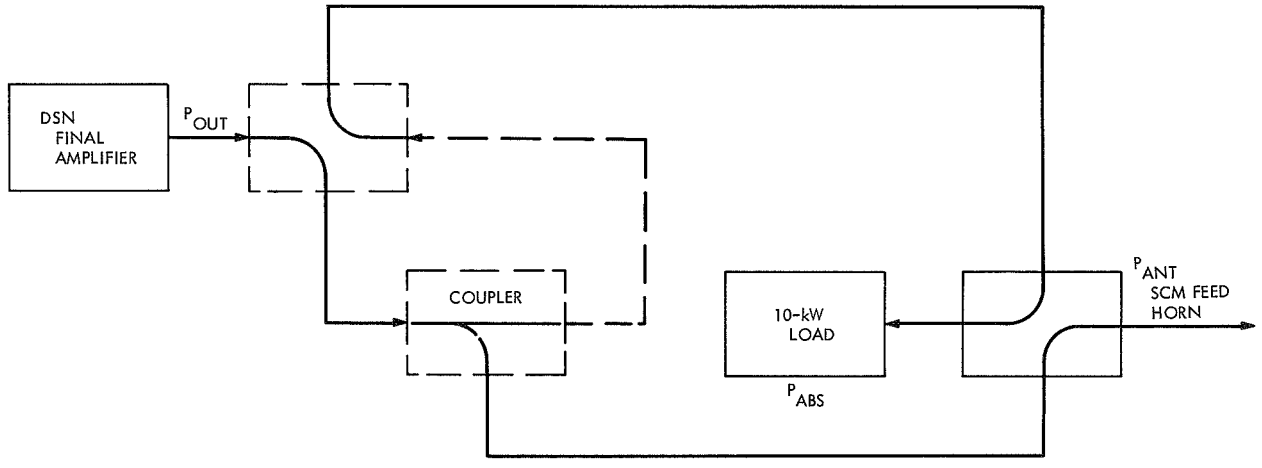

— — — ADDITIONAL EQUIPMENT

MAXIMUM P_{ANT} = 10 kW

P_{OUT} = 10 kW (CONSTANT)

COUPLER FACTOR, dB	P_{ABS}, W	P_{ANT}, W
30	9990	10
20	9900	100
10	9000	1000

Fig. 3. Directional coupler in a standard 85-ft-diam antenna station

couplers previously described. If the device performs as described in the article, its most useable range would certainly be limited to approximately 60 deg of rotation which yields a maximum attenuation of −6 dB. Reference to Fig. 4 shows that the resolution (decibels of attenuation per degree of rotation) is degraded when the rotation exceeds 60 deg. That is, the sensitivity of the device is such that it should be limited to an operational maximum of 0.25 dB/deg of rotation. Given a maximum useable attenuation range of −6 dB, clearly the device is incapable of providing the degree of attenuation necessary to reduce 10 or 20 kW to 10 or 20 W. However, the device should prove to be very useful when used in conjunction with a directional coupler as illustrated in Fig. 5. The combination of a fixed coupler plus the power divider should provide a very accurate and variable (over a 6-dB range) method of obtaining the low power level desired at the antenna.

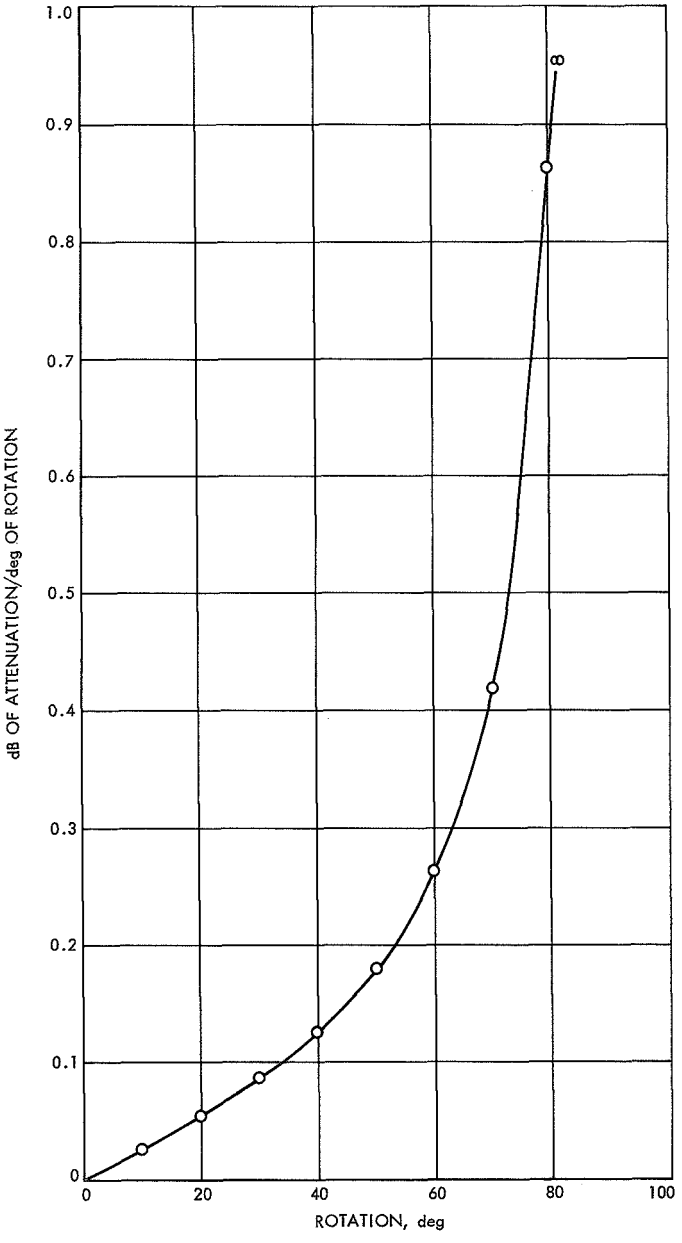

Fig. 4. Decibels of attenuation per degree of rotation for high-power microwave power divider

3. Summary

The configurations proposed above may be summarized in Table 1, which shows the power radiated from the horn using two different directional couplers; with and without the microwave power divider. In Table 1, it is assumed that the maximum attenuation obtained from the power divider is −6 dB. In actual practice, however, this may be increased to as much as −10 dB at 72 deg of rotation, but with a corresponding decrease in resolution, as the curve in Fig. 6 indicates.

It would appear that the optimum configuration for either the 85-ft mutual station or the standard station would be the use of a 20-dB coupler, plus a power divider, as shown in Figs. 1 and 3, respectively. This gives a 25- to 100-W variable output or, with a corresponding degradation in tolerance a variable output of 10 to 100 W.

Consideration should be given to the development of the high-power microwave power divider as described in the attached article. With the proper electromechanical design, the capability to accurately control transmitted power by remote control or automatically by computer would be possible.

Table 1. Station configuration summary

Station configuration	Power at antenna feed horn, W			
	Coupler only		Coupler plus divider	
	30 dB	20 dB	30 dB	20 dB
85-ft-diam antenna mutual station (20 kW)				
Fig. 1 configuration	10	100	2.5 to 10	25 to 100
Fig. 2 configuration	20	200	5 to 20	50 to 200
85-ft standard station (10 kW)				
Fig. 3 configuration	10	100	2.4 to 10	25 to 100

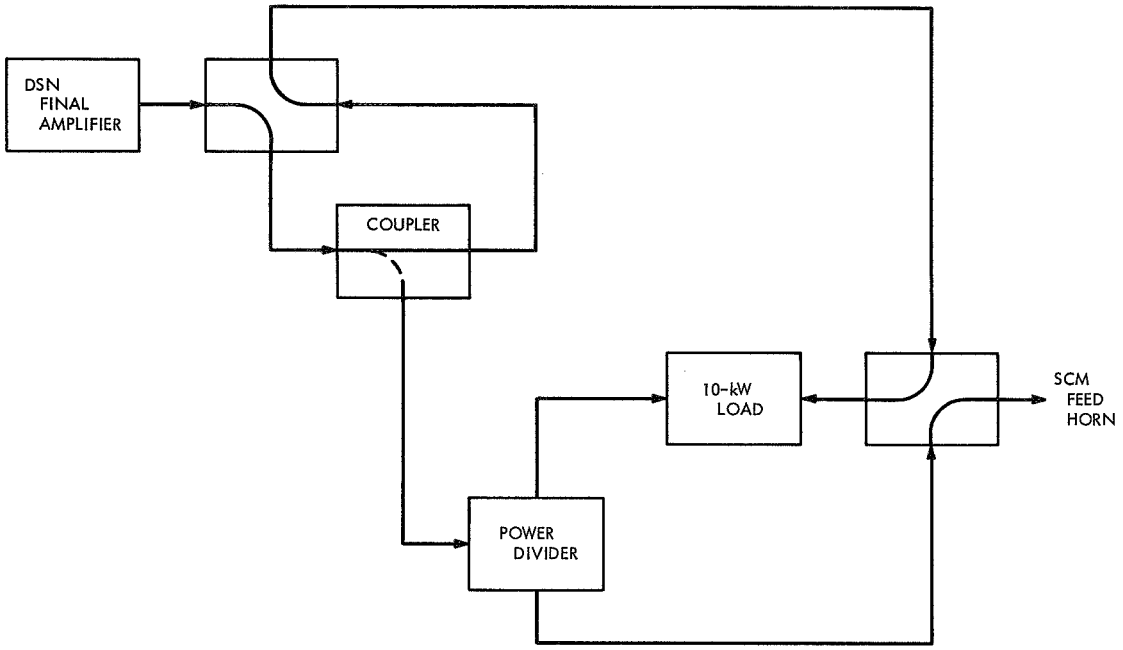

Fig. 5. Directional coupler plus power divider

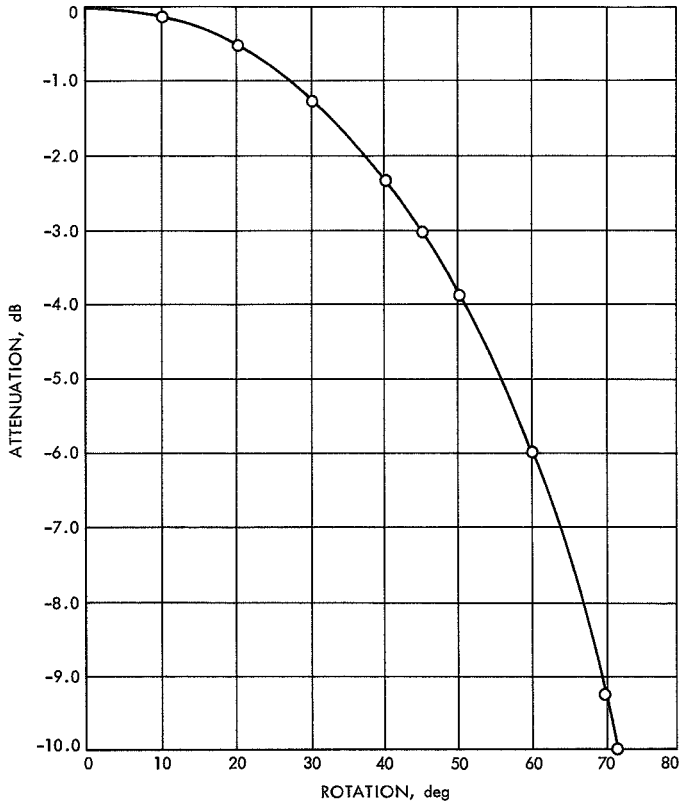

Fig. 6. Attenuation of input power versus degrees of rotation for high-power microwave power divider

D. A New Tropospheric Range Refraction Model,

A. L. Berman

1. Introduction

Atmospheric (tropospheric) refraction can be easily separated into two components. Most analysis lumps the two together; in this report they will be dealt with separately:

$$N = \text{refractivity}$$

$$N = N_d + N_w$$

where

$$N_d = \text{dry component}$$

$$N_w = \text{wet component}$$

Previously, the dry component of range and range rate refraction (signal retardation component) has been assumed to be a linear function of surface refractivity. This appears to be a result of assuming an isothermal atmospheric model and then failing to consider the functional dependence required of the "scale height" by that assumption. Consideration of the hydrostatic equation and the gas law lead inescapedly to the conclusion that range refraction (at least at reasonable elevation angles) is linearly dependent upon surface pressure and not surface refractivity. The derivation of the functional basis of the dry component is presented in *Subsection 2*; in *Subsection 3*, a method of integrating the wet component is presented; and finally, *Subsection 4* describes the errors which would result from the use of the new model—these errors being then compared to current model errors.

2. Dry-Term Derivation

In general, two tropospheric range refraction effects are recognized, namely, decrease in signal propagation velocity and increase in geometrical refracted signal path. The ratio of effect of the latter to the former can be roughly represented as (Ref. 1):

$$\frac{(\Delta R)_R}{(\Delta R)_v} \approx B \cos\theta$$

where

$$(\Delta R)_R = \Delta_R \text{ due to geometrical path}$$

$$(\Delta R)_v = \Delta_R \text{ due to propagation velocity}$$

$$B = \text{inverse scale height, } \text{km}^{-1} \approx 0.1$$

$$\theta = \text{elevation angle}$$

Since the value of $(\Delta R)_R$ can be seen to vary from 0 to 0.1 of the value of $(\Delta R)_v$, it seems reasonable to limit the discussion to the effect of signal velocity retardation only.

The index of refraction for the troposphere is generally considered to be comprised of two separate components, sometimes referred to as the dry (main) and wet components:

$$n = 1 + 10^{-6}N$$

$$N = N_d + N_w$$

$$N_d = 77.6\,\frac{P}{T}$$

$$N_w = 77.6\,(4810)\,\frac{(RH)e_s}{T^2}$$

where

$$T = \text{temperature, °K}$$

$$n = \text{index of refraction}$$

$$N = \text{refractivity}$$

$$P = \text{pressure, mbar}$$

$$RH = \text{relative humidity (\% of 1.0)}$$

$$e_s = \text{saturation vapor pressure, mbar}$$

A cursory examination of the two expressions shows N_w to be in the vicinity of 10% of the value of N_d; for example, in the following case where

$$T = 273°\text{K}$$

$$P = 1000 \text{ mbar}$$

$$RH = 1.0$$

$$e_s(T) = 6.11 \text{ mbar}$$

$$\frac{N_w}{N_d} = 0.1077$$

Thus, it would appear advantageous initially to limit the analysis to the dry component of refractivity.

We begin by considering the physical signal path range as the troposphere is traversed:

$$R = \int_0^s cdt = \int_0^s ds$$

We then consider an apparent refracted range R' with signal velocity v:

$$v = c/n$$

$$R' = \int_0^s cdt' = \int_0^s c\,\frac{ds}{v} = \int_0^s nds$$

so that the range correction ΔR is

$$\Delta R = R' - R = \int_0^s nds - \int_0^s ds$$

$$= \int_0^s (n-1)\,ds$$

$$= 10^{-6}\int_0^s Nds$$

Relating ds to height above the observation point z and elevation angle θ (at least for high elevation angles) we obtain

$$ds \approx \frac{dz}{\sin\theta} = \csc\theta\,dz$$

so that

$$\Delta R \approx 10^{-6}\int_0^z N \csc\theta\,dz$$

However, since what we are really interested in is the dependence of ΔR upon $N(z)$ we will ignore spherical geometry considerations:

$$\Delta R \approx 10^{-6}\csc\theta\int_0^z N(z)\,dz$$

and define

$$\Delta r = \frac{\Delta R}{10^{-6}\csc\theta} \approx \int_0^z N(z)\,dz$$

so that we can evaluate the functional dependence of Δr upon $P_0, T_0, \cdots$, etc.

Typically, in the past this has been handled by assuming that

$$N(z) = N_s \exp(-Bz)$$

where

N_s = surface refractivity

B = constant, inverse scale height in $km^{-1} \approx 0.1$

The total (elevation-independent) refraction effect (considering that the tropospheric-type refraction is nil by 75 km) becomes

$$\Delta r = \int_0^{75} N_s \exp(-Bz)\,dz$$

$$\approx \int_0^{\infty} N_s \exp(-Bz)\,dz$$

$$\approx N_s/B$$

However, this does not seem to be an entirely adequate treatment of the problem. The assumption of an exponential decay refractivity is rooted in the assumption of an isothermal, or constant temperature, troposphere. If we consider this to be true, we would have:

$$T(z) = T_0$$

$$P(z) = P_0\,e^{-Bz}$$

and indeed

$$N(z) = A\frac{P(z)}{T(z)} = \left(A\frac{P_0}{T_0}\right)e^{-Bz}$$

$$= N_s\,e^{-Bz}$$

However, it is easy to show (Ref. 2) that for this to be true, we require

$$B = g/RT_0$$

where

g = gravitational force

R = gas constant

$$\frac{g}{R} = 34.1°\text{C/km}$$

Integrating this expression, we have

$$\Delta r = \int_0^{75} N(z)\,dz \approx \int_0^{\infty} N(z)\,dz$$

$$\Delta r \approx \int_0^\infty A \frac{P_0}{T_0} \exp(-gz/RT_0)\, dz$$

$$\approx \left(A \frac{P_0}{T_0}\right)\left[-\left(\frac{RT_0}{g}\right)\exp(-gz/RT_0)\right]_0^\infty$$

$$\approx A\left(\frac{R}{g}\right)P_0$$

which would lead to the unmistakable conclusion that range refraction is basically linearly dependent upon surface pressure and not surface refractivity.

However, an isothermal atmosphere is a rather poor assumption; a much better idea would be to assume a standard atmosphere profile. For instance, a typical profile would be for a station at a height of h_0 above sea level:

$$0 \leq z \leq (11 - h_0)\ \text{km}$$

$$T(z) = T_0 - \gamma z$$

$$P(z) = P_0\left(\frac{T(z)}{T_0}\right)^{g/R\gamma}$$

$$\gamma = \gamma(T_0) = \left(\frac{T_0 - T_1}{11 - h_0}\right)$$

and

$$(11 - h_0)\ \text{km} \leq z \leq (21 - h_0)\ \text{km}$$

$$T(z) = T_1 = 216.65°\text{K}$$

$$P(z) = P_0\left(\frac{T_1}{T_0}\right)^{g/R\gamma}\exp\left(-\frac{z - [11 - h_0]}{RT_1}g\right)$$

We would then have for the refraction contribution

$$\Delta r = \int_0^z N(z)\, dz$$

$$= \int_0^{11-h_0} A\frac{P_0}{T_0}\left(\frac{T_0 - \gamma z}{T_0}\right)^{g/R\gamma - 1} dz$$

$$+ \int_{11-h_0}^{21-h_0} A\frac{P_0}{T_0}\left(\frac{T_1}{T_0}\right)^{g/R\gamma}$$

$$\times \exp\left(-\frac{z - [11 - h_0]}{RT_1}g\right)dz$$

We allow $(21 - h_0)\text{km} \to \infty$ (because of the small contribution above 21 km) so that

$$\Delta r \approx \frac{AP_0}{T_0}\int_0^{11-h_0}\left(\frac{T_0 - \gamma z}{T_0}\right)^{g/R\gamma - 1} dz$$

$$+ \frac{AP_0}{T_0}\int_{11-h_0}^\infty \left(\frac{T_1}{T_0}\right)^{g/R\gamma}\exp\left(-\frac{z - [11 - h_0]}{RT_1}g\right)dz$$

$$\approx AP_0\left(\frac{R}{g}\right)\left[1 - \left(\frac{T_1}{T_0}\right)^{g/R\gamma}\right] + AP_0\left(\frac{R}{g}\right)\left(\frac{T_1}{T_0}\right)^{g/R\gamma}$$

$$\approx AP_0\left(\frac{R}{g}\right)\left[1 - \left(\frac{T_1}{T_0}\right)^{g/R\gamma} + \left(\frac{T_1}{T_0}\right)^{g/R\gamma}\right]$$

$$\approx AP_0\left(\frac{R}{g}\right)$$

Finally, it can be shown quite easily that this result will occur regardless of the temperature/pressure distribution by merely examining the hydrostatic equation and the perfect gas law:

$$dp = -\rho g\, dz \qquad \text{(hydrostatic equation)}$$

and

$$P = \rho RT \qquad \text{(gas law)}$$

$$N(z) = A\frac{P_{(z)}}{T_{(z)}} = A\frac{\rho RT}{T} = A\rho R$$

$$= A\left(-\frac{1}{g}\frac{dp}{dz}\right)R$$

$$\Delta r \approx \int_0^\infty N(z)\, dz$$

$$\approx -\int_0^\infty \left(A\frac{1}{g}\frac{dp}{dz}\right)R\, dz$$

$$\approx -\int_{P_0}^0 \frac{AR}{g}\, dp = \frac{AR}{g}P_0$$

Or, once again:

$$\Delta r \approx A\left(\frac{R}{g}\right)P_0$$

3. Integration of Wet Term

In *Subsection 2*, it was indicated that a scaled range refraction Δr could be calculated as

$$\Delta r = \int_z^0 N(z)\, dz$$

where N could be split into a wet and dry component:

$$N = N_d + N_w$$

The quantity $(\Delta r)_d$ was then evaluated according to

$$(\Delta r)_d = \int_0^z N_d(z)\, dz$$

We now wish to evaluate a similar expression for the wet component:

$$(\Delta r)_w = \int_0^z N_w(z)\, dz$$

From SPS 37-45, Vol. IV, pp. 270–276, we have the following expression for N_w:

$$N_w = \left(\frac{(RH)C_1C_2}{T^2}\right) 10^{[(K_1T-K_2)/(T-C)]}$$

$$= \left(\frac{(RH)C_1C_2}{T^2}\right) \exp\left[\frac{(K_1T - K_2)\ln(10)}{T - C}\right]$$

$$= \left(\frac{(RH)C_1C_2}{T^2}\right) \exp\left(\frac{AT - B}{T - C}\right)$$

where

$C_1 = 77.6$

$C_2 = 29341.0$

T = temperature, °K

$A = K_1 \ln(10) = 7.4475 \ln(10)$

$B = K_2 \ln(10) = 2034.28 \ln(10)$

$C = 38.45$

RH = relative humidity (% of 1.0)

To perform (approximately) the integration

$$(\Delta r)_w = \int_0^z N_w(z)\, dz$$

we need two relationships, namely:

$$T = T(z)$$

$$RH = RH(z)$$

and an upper bound for z. The most difficult task is to determine how relative humidity might depend upon the surface value and altitude. Perhaps the best assumption would be that

$$RH(z) = RH_s$$

where

RH_s = the relative humidity at surface

At least this would be reasonable at low heights, where by far the greatest contribution to refraction (wet component) occurs. As concerns temperature, we can assume a constant negative lapse rate to the (approximate) tropopause ($z \approx [11 - h_0]$km):

$$T(z) = T_0 - \gamma z$$

$$\gamma = \gamma(T_0) = \frac{T_0 - T_1}{11 - h_0}$$

where

T_0 = surface temperature, °K

z = height above station, km

h_0 = station height, km

$T_1 = 216.65$°K

We can now transform our integral accordingly:

$$dt = -\gamma\, dz$$

$$(\Delta r)_w = \int_0^z N_w(z)\, dz$$

$$= \int_{T_0}^{T_1} \frac{(RH_s)C_1C_2}{T^2} \exp\left(\frac{AT - B}{T - C}\right)\left(-\frac{dT}{\gamma}\right)$$

$$= -\left\{\frac{C_1C_2(RH)_s}{\gamma(T_0)}\right\} \int_{T_0}^{T_1} \frac{1}{T^2} \exp\left\{\frac{AT - B}{T - C}\right\} dT$$

Thus we wish to evaluate

$$F(T_0) = \int_{T_0}^{T_1} \frac{dT}{T^2} \exp\left(\frac{AT - B}{T - C}\right)$$

If we make the substitution

$$Y = \frac{AC - B}{T - C}$$

we would then have

$$\exp\left(\frac{AT - B}{T - C}\right) = \exp(A + Y) = \exp(A)\exp(Y)$$

$$T = \frac{AC - B + CY}{Y}$$

$$dT = \frac{B - AC}{Y^2}\, dY$$

$$\frac{dT}{T^2} = \frac{B - AC}{Y^2}\, dY \left(\frac{Y^2}{[AC - B + CY]^2}\right)$$

and letting

$$Y_0 = \frac{AC - B}{C}$$

$$\frac{dT}{T^2} = \frac{1}{(B - AC)}\left(\frac{dY}{(1 + Y/Y_0)^2}\right)$$

so that

$$F(T_0) = \int_{T_0}^{T_1} \frac{dT}{T^2} \exp\left(\frac{AT - B}{T - C}\right)$$

$$= \left(\frac{\exp(A)}{B - AC}\right) \int_{Y(T_0)}^{Y(T_1)} \frac{\exp(Y)\, dY}{(1 + Y/Y_0)^2}$$

For the most extreme possible range of temperatures, we would have for the variation in the y-dependent terms:

$$216 < T < 316$$

$$-22.67 \simeq Y \simeq -14.50$$

$$1.4 \times 10^{-10} \gtrsim \exp(Y) \gtrsim 5 \times 10^{-7}$$

$$1.22 \gtrsim (1 + Y/Y_0) \gtrsim 1.15$$

Since the variation in the denominator is almost nil compared to the variation in the exponential term, we can approximate the integral:

$$\int_{Y(T_0)}^{Y(T_1)} \frac{\exp(Y)\, dY}{(1 + Y/Y_0)^2} \approx \frac{\exp(Y)}{(1 + Y/Y_0)^2}\Bigg|_{Y(T_0)}^{Y(T_1)}$$

Furthermore, since

$$\frac{\exp[Y(T_1)]}{\exp[Y(T_0)]} \approx 3 \times 10^{-4}$$

we can ignore the upper limit:

$$F(T_0) \approx -\frac{\exp[Y(T_0)]}{[1 + Y(T_0)/Y_0]^2}\left(\frac{\exp(A)}{B - AC}\right)$$

$$\approx -\frac{\exp\left(\frac{AC - B}{T_0 - C}\right)}{\left(1 + \frac{C}{T_0 - C}\right)^2}\left(\frac{\exp(A)}{B - AC}\right)$$

$$\approx -\frac{\left(1 - \frac{C}{T_0}\right)^2}{(B - AC)} \exp\left(\frac{AT_0 - B}{T_0 - C}\right)$$

and finally

$$(\Delta r)_w \approx \left[\frac{C_1 C_2 (RH)_s}{\gamma(T_0)}\right]\left[\frac{\left(1 - \frac{C}{T_0}\right)^2}{B - AC}\right] \exp\left(\frac{AT_0 - B}{T_0 - C}\right)$$

This result, when combined with the expression for $(\Delta r)_d$ presented in *Subsection 2* should give the total functional dependence of range (and range rate) refraction upon the surface variables P_0, T_0, and $(RH)_s$.

4. Error Analysis

a. Combined refraction model. In *Subsection 2* it was shown that the current so-called exponential refractivity model was predicated upon a faulty assumption, and a more correct formulation for range refraction was detailed. We are here concerned with the two separate, additive components of refractivity, the so-called wet and dry terms:

$$N(z) = N_d(z) + N_w(z)$$

with

$$N_d(z) = -\frac{AR}{g}\left(\frac{dP}{dz}\right)$$

and

$$N_w(z) = \frac{(RH)C_1C_2}{T^2}\,10\left(\frac{K_1T - K_2}{T - C}\right)$$

and where

$A = 77.6$

$R =$ gas constant

$g =$ gravity

$p =$ pressure

$RH =$ relative humidity

$C_1 = 77.6$

$C_2 = 29341.0$

$T =$ temperature

$K_1 = 7.4475$

$K_2 = 2034.28$

$C = 38.45$

Integration of the major, or dry, term, as shown in *Subsection 2*, is quite simple, namely:

$$\int_0^\infty N_d(z)\,dz = AP_0\left(\frac{R}{g}\right)$$

where

$P_0 =$ surface pressure

Whereas, integration of the wet term is far more complicated, but, with certain assumptions, can be shown (*Subsection 3*) to be approximately equal to

$$\int_0^\infty N_w(z)\,dz \cong \left[\frac{C_1C_2(RH_s)}{\gamma}\right]\left[\frac{\left(1 - \frac{C}{T_0}\right)^2}{B - AC}\right] \times \exp\left(\frac{AT_0 - B}{T_0 - C}\right)$$

where

$\gamma =$ temperature lapse rate

$(RH)_s =$ surface relative humidity

$T_0 =$ surface temperature

When combined, we have for the total zenith range refraction, as a function of surface meteorological parameters and temperature lapse rate:

$$(\Delta r) \cong AP_0\left(\frac{R}{g}\right) + \left[\frac{C_1C_2(RH)_s}{\gamma}\right]\left[\frac{\left(1 - \frac{C}{T_0}\right)^2}{B - AC}\right] \times \exp\left(\frac{AT_0 - B}{T_0 - C}\right)$$

which can be compared to the current expression:

$$(\Delta r) = \frac{N_s}{B} = AP_0\left(\frac{1}{T_0B}\right)$$

The assumptions required to perform the integration of the wet term are

$$T(z) = T_0 - \gamma z$$

and

$$RH(z) = (RH)_s$$

Thus it should be kept in mind that the expression for the integrated wet term is accurate only to the extent that these assumptions prove true. The accuracy ramifications embodied in the above assumptions will be examined in detail. Preparatory to this, however, it seems timely to present a description of prevailing meteorological conditions.

b. Description of temperature profiles. The region for which we are interested in defining the functional dependence of temperature upon altitude is from the station height to the tropopause, or roughly, 0–11 km. At the tropopause, the temperature is approximately −55°C, and by this temperature wet refractivity is nil. It is fortunate that many of the station sites are meteorologically similar, i.e., temperate, semi-arid, and not in proximity to any large bodies of water. For climates

such as these, we can identify two basic types of temperature profiles; a summer-type profile (warm and usually clear) and a winter-type profile (cold and often cloudy). The summer-type profile is the simpler of the two, and is shown in Fig. 1. Generally, over a period of days, the slope and T_0 remain reasonably constant, although near the ground, there is a diurnal swing from night inversion to day ground heating and back. The winter-type profiles are more complicated in that inversions occur up to a far greater altitude, and instead of consisting of just one main segment, they are typically comprised of several segments (Fig. 2).

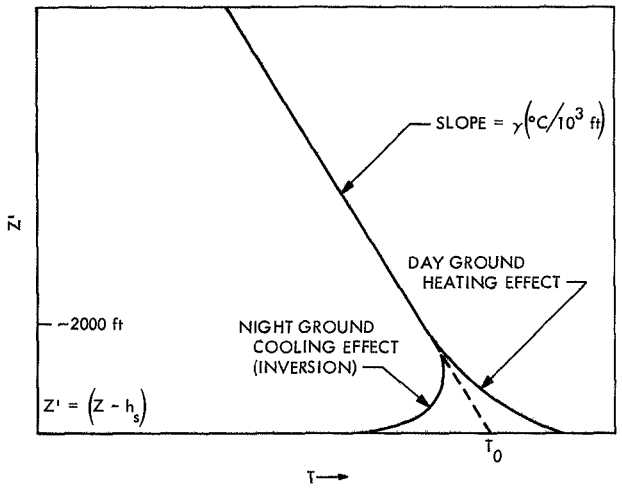

Fig. 1. Summer-type profile

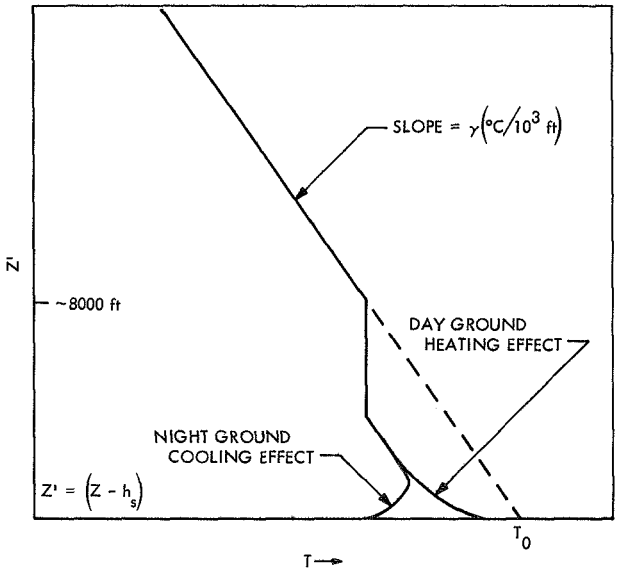

Fig. 2. Winter-type profile

c. Description of relative humidity profiles. After examining a number of relative humidity profiles, one is forced to conclude that there appears to exist no particular functional dependence of relative humidity upon altitude (such as exists with temperature); perhaps the most that can be inferred from the profiles viewed in this report, is that relative humidity seems (but only tenuously!) to remain more constant with altitude during summer-type weather than during winter-type weather (although this would have a good implication, as, in general, the summer wet-term contribution is two to three times the size of the winter contribution). Some examples of relative humidity profiles encountered are shown in Fig. 3. As one might guess, the uncertainties connected with relative humidity profiles produce the largest model errors; however, the use of the assumption:

$$RH(z) = RH_s$$

does not lead to errors as bad as one might at first be inclined to think, because most of the wet-term contribution is concentrated at low altitudes where often the relative humidity has not yet changed as appreciably as it frequently has at the higher altitudes.

d. Meteorological data necessary to implement the proposed model. We have derived the expression for the total (zenith) range refraction as:

$$(\Delta r) = AP_0\left(\frac{R}{g}\right) + \left[\frac{C_1C_2(RH)_s}{\gamma}\right]\left[\frac{B - AC}{\left(1 - \frac{C}{T_0}\right)}^2\right] \times \exp\left(\frac{AT_0 - B}{T_0 - C}\right)$$

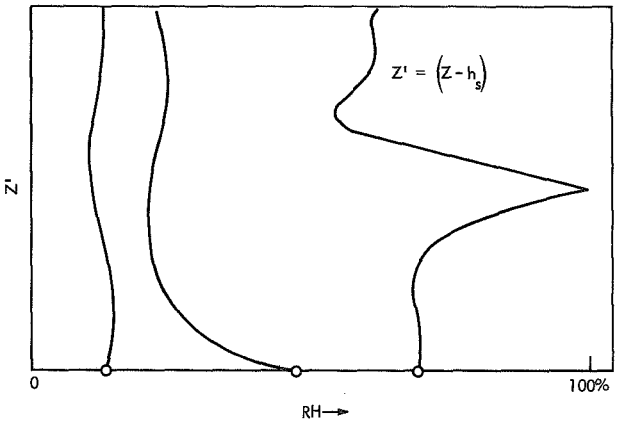

Fig. 3. Relative humidity profiles

To evaluate this expression we require the meteorological inputs:

P_0 = surface pressure

γ = temperature lapse rate

T_0 = extrapolated surface temperature

$(RH)_s$ = surface relative humidity

Basically, the proposed implementation being suggested here is that P_0 and $(RH)_s$ be supplied from frequent (several times daily) samplings at the station, while γ and T_0 be extracted from less frequent (perhaps every several days) atmospheric soundings from any available source in the vicinity (within 100 miles) of the station. When considering this proposal, it should be borne in mind that the dry term, which depends only on surface pressure, represents about 90% of the total tropospheric refraction; thus, even if atmospheric soundings do not prove readily accessible to most stations, γ and T_0 could probably be modeled on a seasonal basis without resulting in too great a loss of accuracy. More specifically then, the data requirements to support the model are defined as follows:

Dry component. Surface pressure measurements at the station would be used to compute the dry-term refraction contribution; due to the slowly varying nature of pressure (barring tornadoes, etc.), measurements every 6 h would be the most frequent that could possibly be needed.

Wet component. Atmospheric soundings would be the best source for the determination of γ and T_0; however, this requirement can be very loosely structured. For instance, the upper troposphere appears to change only slowly, such that soundings might only be required every several days; secondly, since the upper troposphere varies (relatively) slowly horizontally,[2] any source of soundings within perhaps 100 miles should be adequate. For instance, for the Goldstone DSCC, the atmospheric soundings taken at Edwards A.F.B. would seem to amply satisfy this requirement. As already mentioned, if soundings are just not available, T_0 and γ can probably be seasonally modeled without too great a degradation in accuracy. Finally, surface relative humidity measurements at the station would be required. Although this is a rapidly changing parameter, the assumption of constant relative humidity (with altitude) is already quite inaccurate, such that perhaps one "average" surface relative humidity sample per 6-h period would suffice.

*e. **Error analysis.*** When considering the implementation of the scheme proposed here, four major sources of error are in evidence: temperature lapse rate, extrapolated surface temperature, local ground temperature effects (night inversions and day ground-heating), and a non-constant relative humidity. To test the scheme, five days were chosen which represented both seasonal types (two winter-type profiles, two summer-types, and one in-between type). For each day, atmospheric sounding data from Edwards A.F.B. was used to construct two separate sets of temperature and relative humidity profiles, one in the late night and one in the afternoon, so as to maximize distortions due to local ground effects. The days chosen were in December, February, April, August, and September. See Fig. 4 a through j, which will hereafter be referred to as cases 1 through 10. A discussion of the various error magnitudes follows:

Errors in γ and T_0. To approximate the magnitude of the possible errors in slope γ and in T_0, the differences in the graphically computed values of γ and T_0 over the roughly 12-h separation for each day were calculated. These values are given in Table 1.

Table 1. Errors in $\Delta\gamma$ and ΔT_0

Error	Dec.	Feb.	April	Aug.	Sept.
$\Delta\gamma$, °C/10³ ft	0.100	0.025	0.073	0.166	0.017
ΔT_0, °C	1.0	1.0	3.0	2.0	1.0

The resulting average differences are

$$\Delta\gamma \approx 0.076°C/10^3 \text{ ft}$$

$$\Delta T_0 \approx 1.6°C$$

Enlarging these figures somewhat, e.g.,

$$\Delta\gamma \approx 0.1°C/10^3 \text{ ft}$$

$$\Delta T_0 \approx 2.0°C$$

we might consider that these values approximate the uncertainties inherent to the determination of γ and T_0 from atmospheric soundings taken every several days.

[2]Smyth, J. B., *Radio Meteorology at JPL Goldstone Station* (final report), p. 5, July 1965 (JPL internal document).

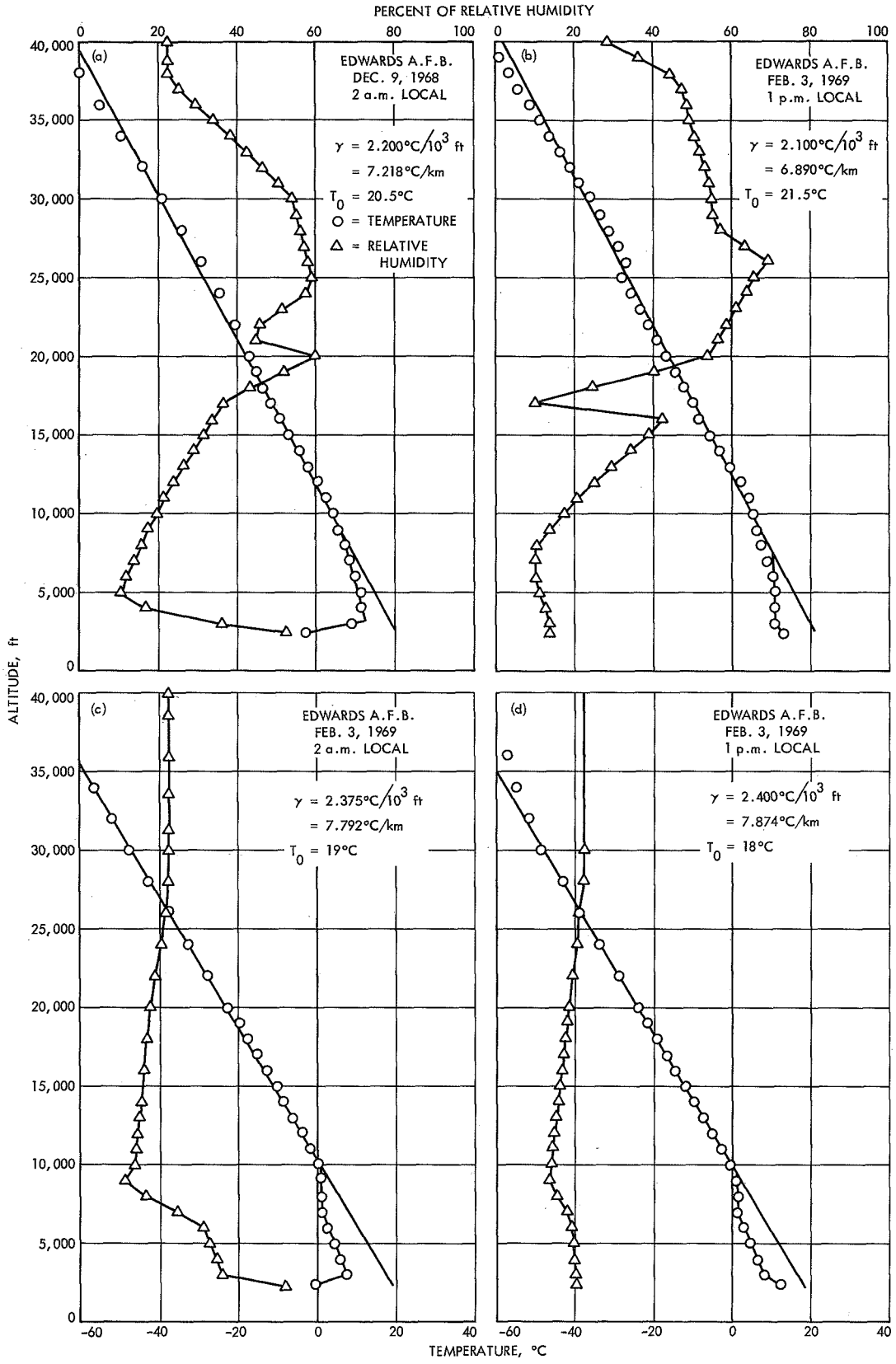

Fig. 4a to d. Temperature and relative humidity versus altitude, cases 1–4

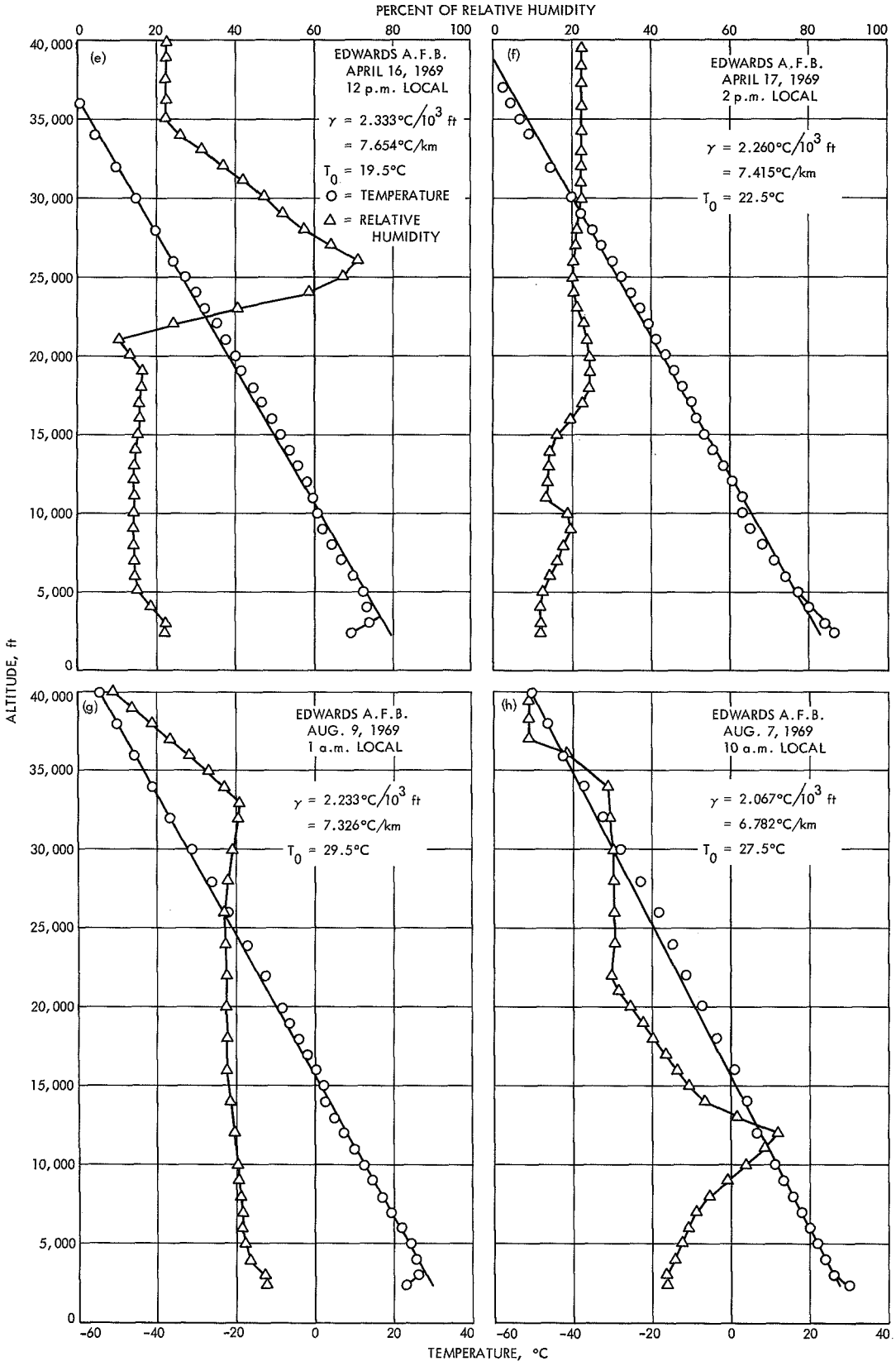

Fig. 4e to h. Temperature and relative humidity versus altitude, cases 5–8

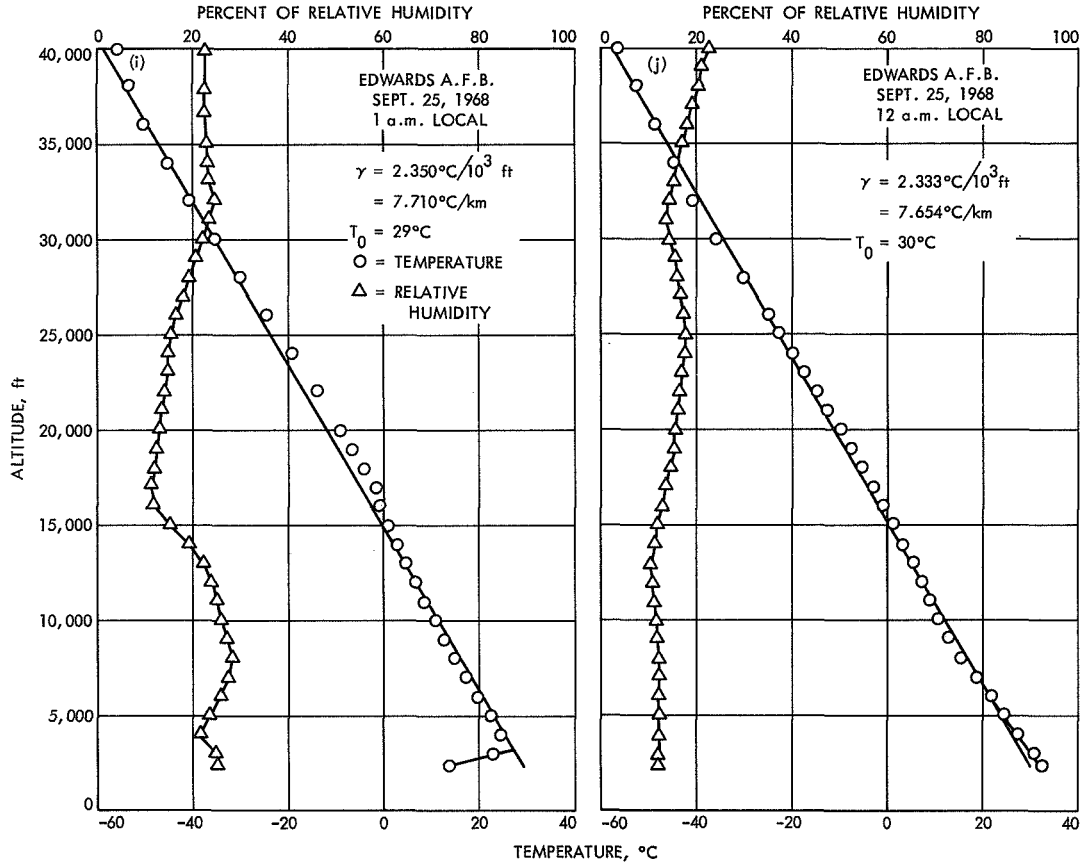

Fig. 4i to j. Temperature and relative humidity versus altitude, cases 9–10

The above values would have produced uncertainties in Δr_w (wet-term refraction, in centimeters) for each of the ten cases as shown in Table 2.

The average uncertainties are

$$\Delta T_0 \approx 1.20 \text{ cm}$$

$$\Delta\gamma \approx 0.48 \text{ cm}$$

Combining these uncertainties in an rms sense, we would have a composite uncertainty due to errors in γ and T_0 of

$$\sum_{\text{rms}}^{\gamma, T_0} \text{errors} \approx 1.30 \text{ cm}$$

Errors due to local ground temperature effects. Using the temperature profiles in cases 1 to 10, the differences between the actual near-ground temperature profile and the extrapolated temperature profile to T_0 were calculated. These differences, in centimeters of wet-term refraction, are given in Table 3. This gives an average error magnitude of

$$|\text{Error}| \text{ ground temperature effects} \approx 0.66 \text{ cm}$$

Errors due to assumption of constant relative humidity. Using the relative humidity profiles in cases 1 to 10, the differences in wet-term refraction due to the differences between the actual relative humidity profile versus an assumed constant relative humidity (equal to the surface relative humidity) were calculated. These differences are given in Table 4. The average error magnitude is

$$|\text{error}| \text{ constant relative humidity assumption} \cong 2.32 \text{ cm}$$

Thus, the assumption of constant relative humidity leads to the largest model errors.

Combined errors of proposed scheme. Considering all the errors to be independent (which to varying degrees

Table 2. Uncertainties in Δr_w

Uncertainty in Δr_w	Case No.									
	1	2	3	4	5	6	7	8	9	10
Due to $\Delta\gamma$	0.66	0.18	0.60	0.23	0.27	0.18	1.05	0.85	0.54	0.27
Due to ΔT_0	1.74	0.48	1.56	0.58	0.68	0.44	2.52	2.04	1.32	0.64

Table 3. Differences in Δr_w due to ground temperature effects

Case No.									
1	2	3	4	5	6	7	8	9	10
1.5 cm	0.7 cm	2.3 cm	0.9 cm	0.4 cm	−0.1 cm	−0.2 cm	0.0 cm	0.3 cm	−0.2 cm

Table 4. Differences in wet-term refraction due to constant RH

Case No.									
1	2	3	4	5	6	7	8	9	10
7.0 cm	−1.6 cm	5.8 cm	0.7 cm	1.2 cm	−1.0 cm	2.7 cm	−2.3 cm	0.8 cm	−0.1 cm

they are not), we would have a total rms error of

$$\sum_{\text{rms}}^{\text{all}} \text{errors} \approx 2.74 \text{ cm}$$

Or simply summing the absolute values of the various errors, we would have

$$\sum^{\text{all}} |\text{errors}| \approx 4.66 \text{ cm}$$

Both figures are considerably less than what is seemingly being obtained in the way of accuracy with the current model.

Comparison with current models. Although the above figures point to the magnitude of the errors which might result if the proposed model was implemented in conjunction with the data sources already described, perhaps the best way to illustrate the increase in accuracy would be to compare the errors which would have been obtained via the new scheme to those which would result from using the current (incorrect) model. First, we will assume an average pressure (at Edwards A.F.B.) of

$$P_0 = 900 \text{ mbar}$$

which will produce a dry-term contribution (to zenith range refraction) of

$$AP_0\left(\frac{R}{g}\right) = 204.8 \text{ cm}$$

Graphically, the (actual) wet-term contributions have been calculated for each of the ten cases, and, when added to the aforementioned dry-term contribution, produce the resultant total refraction shown in Table 5.

The wet-term and total refraction which would have resulted using the proposed scheme (i.e., exhibiting errors due to local ground temperature effects and assumption of constant relative humidity) is shown in Table 6.

As we have seen in *Subsection 2*, the current "exponential decay refractivity" model leads to an expression for total refraction of

$$(\Delta r) = N_s/B$$

Presently, computer programs such as the Orbit Determination Program (ODP), PREDICTS, etc., allow only

Table 5. Total refraction of wet-term and dry-term contributions

Refraction	Case No.									
	1	2	3	4	5	6	7	8	9	10
Wet, cm	4.8	4.6	3.8	2.9	3.7	4.6	18.1	19.3	9.7	5.7
Total, cm	209.6	209.4	208.6	207.7	208.5	209.4	222.9	224.1	214.5	210.5

Table 6. Wet-term and total refraction using proposed scheme

Refraction	Case No.									
	1	2	3	4	5	6	7	8	9	10
Wet, cm	13.3	3.7	11.9	4.5	5.3	3.5	21.0	17.0	10.8	5.4
Total, cm	218.1	208.5	216.7	209.3	210.1	208.3	225.8	221.8	215.6	210.2

Table 7. Surface refractivity and resultant refraction

Refractivity	Case No.									
	1	2	3	4	5	6	7	8	9	10
Actual N_s, cm	272	253	271	259	259	250	293	305	262	252
N_s/B, cm	191.5	178.5	190.9	182.1	182.5	176.3	206.0	214.7	184.4	177.7

Table 8. Comparison of refraction scheme errors

Model	Case No.									
	1	2	3	4	5	6	7	8	9	10
Proposed Scheme	8.5	− 0.9	8.1	1.6	1.6	− 1.1	2.9	− 2.3	1.1	− 0.3
Current and actual N_s	−18.1	−30.9	−17.7	−25.6	−26.0	−33.1	−16.9	− 9.4	−30.1	−32.8
Current and fixed N_s	−31.4	−31.2	−30.4	−29.5	−30.3	−31.2	−44.7	−45.9	36.3	−32.3

fixed values for surface refractivity and inverse scale height. The values typically in use are

$$N_s = 253 \quad \text{(Goldstone DSCC yearly average)}$$

$$B = 0.142$$

leading to a total refraction of

$$N_s/B = 178.2 \text{ cm}$$

However, we can take the current (incorrect) model one step further and calculate the actual surface refractivity and resultant refraction for each of the ten cases (Table 7).

Finally, differencing the current model with constant refractivity, the current model with actual surface refractivity, and the proposed scheme, all with the actual refractivity (graphically/numerically obtained), we would have the results listed in Table 8.

The following average error magnitudes would result:

Proposed scheme	= 2.8 cm
Current model with N_s actual	= 24.1 cm
Current model with N_s fixed	= 34.3 cm

If the theoretical basis for the new formulation as derived in *Subsections 2* and *3* is correct, then use of the here-proposed scheme would seem to offer the following advantages:

(1) Decrease in total (zenith) range refraction error of up to an order of magnitude.

(2) Less need for station meteorological data samplings than is presently envisioned in Tracking System Analytical Calibration (TSAC) documentation.

References

1. Rowlandson, L. G., *Simple Analytical Functions Which Provide Magnitude of Range and Angle Errors for Propagation in an Exponential Atmosphere*, U.S. Air Force, Hanscom Field, Bedford, Mass., Jan. 19, 1968.

2. Hess, S. L., *Introduction to Theoretical Meteorology*, Holt, Rinehart & Winston, Inc., New York, 1959.